

Enhancing Drug Delivery for Overcoming Angiogenesis and Improving the Phototherapy Efficacy of Glioblastoma by ICG-Loaded Glycolipid-Like Micelles

This article was published in the following Dove Press journal:
International Journal of Nanomedicine

Yupeng Liu¹
Suhuan Dai¹
Lijuan Wen^{1,2}
Yun Zhu³
Yanan Tan³
Guoxi Qiu¹
Tingting Meng¹
Fangying Yu¹
Hong Yuan¹
Fuqiang Hu¹

¹College of Pharmaceutical Science, Zhejiang University, Hangzhou 310058, People's Republic of China; ²National Engineering Research Center for Modernization of Traditional Chinese Medicine - Hakka Medical Resources Branch, School of Pharmacy, Gannan Medical University, Ganzhou 342700, People's Republic of China; ³Ocean College, Zhejiang University, Zhoushan 316021, Republic of China

Background: Phototherapy is a potential new candidate for glioblastoma (GBM) treatment. However inadequate phototherapy due to stability of the photosensitizer and low target specificity induces the proliferation of neovascular endothelial cells for angiogenesis and causes poor prognosis.

Methods: In this study, we constructed c(RGDfk)-modified glycolipid-like micelles (cRGD-CSOSA) encapsulating indocyanine green (ICG) for dual-targeting neovascular endothelial cells and tumor cells, and cRGD-CSOSA/ICG mediated dual effect of PDT/PTT with NIR irradiation.

Results: In vitro, cRGD-CSOSA/ICG inhibited cell proliferation and blocked angiogenesis with NIR irradiation. In vivo, cRGD-CSOSA/ICG exhibited increased accumulation in neovascular endothelial cells and tumor cells. Compared with that of CSOSA, the accumulation of cRGD-CSOSA in tumor tissue was further improved after dual-targeted phototherapy pretreatment. With NIR irradiation, the tumor-inhibition rate of cRGD-CSOSA/ICG was 80.00%, significantly higher than that of ICG (9.08%) and CSOSA/ICG (42.42%). Histological evaluation showed that the tumor vessels were reduced and that the apoptosis of tumor cells increased in the cRGD-CSOSA/ICG group with NIR irradiation.

Conclusion: The cRGD-CSOSA/ICG nanoparticle-mediated dual-targeting phototherapy could enhance drug delivery to neovascular endothelial cells and tumor cells for anti-angiogenesis and improve the phototherapy effect of glioblastoma, providing a new strategy for glioblastoma treatment.

Keywords: angiogenesis, dual-targeting, glycolipid-like micelles, phototherapy, glioblastoma

Introduction

Glioblastoma (GBM) is one of the most common intracranial malignant tumors in adults.^{1,2} It is highly lethal and prone to recur and regenerate.^{3,4} Though surgical treatment, radiotherapy and chemotherapy have made some progress in recent years, the prognosis of GBM patients is dismal due to serious systemic toxicity and side effects^{5,6} and the median survival time is generally less than 14 months.⁷ Therefore, it is urgent to find new effective treatments. Phototherapy, including photodynamic therapy (PDT) and photothermal therapy (PTT), is a new noninvasive local treatment.^{8,9} It has attracted extensive attention in the field of GBM treatments, due to its high efficacy and

Correspondence: Fuqiang Hu
College of Pharmaceutical Science,
Zhejiang University, 866 Yuhangtang
Road, Hangzhou 310058, People's
Republic of China
Tel/Fax +86-571-88208439
Email hufq@zju.edu.cn

low toxicity and side effects.¹⁰ Keyvan Rad et al¹¹ reported folate-conjugated gold-photoactive polymer nanoparticles and combined PDT/PTT for GBM targeting treatment. Dixit¹² used dual receptor-targeted theranostic nanoparticles for GBM effective therapy via PDT.

However, studies have increasingly found that inadequate phototherapy aggravates the degree of hypoxia in solid tumors.¹³ This causes the release of pro-angiogenic factors, such as vascular endothelial growth factor (VEGF) by hypoxia tolerant tumor cells,¹⁴ which can trigger the proliferation of neovascular endothelial cells for angiogenesis.¹⁵ The invasive growth of GBM depends on the degree of tumor vascularization¹⁶ as tumor vessels provide sufficient nutrition for GBM growth.¹⁷ Moreover, compared with normal blood vessels, the tumor vessels are highly permeable and the basement membrane is incomplete, which provides good conditions for GBM invasion and metastasis, thus causing poor prognosis.^{18,19} Therefore, tumor vessel proliferation leads to decreased phototherapy efficacy.²⁰ Currently, antibodies or small molecule inhibitors are often combined with phototherapy^{21,22} to overcome these disadvantages. However, the efficacy of antibodies and small molecule inhibitors is low and temporary.²³ In addition, repeated administration is often leads to drug resistance.^{24,25} Therefore, a new treatment to solve the problem of disordered angiogenesis during GBM phototherapy is urgently needed.

The mechanisms of angiogenesis are complex, including activation and proliferation of neovascular endothelial cells, degradation and remodeling of the extracellular matrix, change in vascular permeability, and generation and remodeling of new blood vessels.^{26,27} Inhibiting a critical stage such as proliferation of neovascular endothelial cells may suppress the disordered angiogenesis caused by GBM phototherapy. Integrin $\alpha_v\beta_3$ is one of the adhesion molecules²⁸ that is highly expressed on the surface of both neovascular endothelial cells and U87 MG cells.^{29,30} Cyclic peptide c(RGDfk) could bind to integrin $\alpha_v\beta_3$ specifically,³¹ which modifies the surface of the drug delivery system and could be used to target HUVECs and U87 MG cells.

Moreover, selecting a high-energy efficiency photosensitizer in the process of phototherapy is also important. Indocyanine green, which is an FDA-approved photosensitizer that can be used for clinical treatments,³² has a long excitation wavelength, good tissue penetration and low toxicity.³³ Indocyanine green can produce a double effect of PDT/PTT to induce apoptosis and necrosis of cells with near-infrared (NIR) irradiation.³⁴ However, the application of indocyanine green in tumor phototherapy is limited,

because it is extremely unstable and easily degrades when exposed to light. Moreover, it is prone to self-aggregation in aqueous solution, leading to poor uptake by cells.^{35,36} Studies have been reported that nanoparticles could enhance drug stability and increase drug accumulation in target cells. High-dose photosensitizer would inhibit the proliferation of neovascular endothelial cells for blocking angiogenesis, and dual-targeted phototherapy could destroy the structure of tumor vessels to enhance drug delivery. Therefore, designing a suitable drug delivery systems is necessary to improve the efficacy of phototherapy treatment of GBM.

In this study, glycolipid-like polymer micelles (CSOSA), constructed by grafting stearic acid and chitosan exhibit low toxicity, easy chemical modification and biodegradability, were modified with a cyclic polypeptide c(RGDfk) as dual-targeted nanocarriers (cRGD-CSOSA). Hydrophobic indocyanine green (ICG) was encapsulated in the hydrophobic core of cRGD-CSOSA. The micellar structure of cRGD-CSOSA could increase the stability of ICG in aqueous solution to enhance the ability of reactive oxygen species (ROS) production. With cRGD modification, cRGD-CSOSA exhibited an increased accumulation in neovascular endothelial cells and tumor cells, the high-dose photosensitizers inhibited the proliferation of neovascular endothelial cells for blocking angiogenesis, and the dual-targeted phototherapy destroyed the structure of tumor vessels for enhancing drug delivery. Therefore, nanoparticles further accumulated in the tumor cells, which promoted apoptosis and necrosis with NIR irradiation. Additionally, the dualeffect of PDT/PTT mediated by ICG could synergistically improve the phototherapy efficacy of GBM (Figure 1). Furthermore, the tumor suppression effect of cRGD-CSOSA/ICG with NIR irradiation was investigated using a xenografted GBM mouse model.

Materials and Methods

Materials

Chitosan oligosaccharide (CSO) with an average molecular weight of 18.0 *kDa* was obtained by enzymatic degradation of chitosan, and Gel Permeation Chromatography (GPC) method was used to confirm the modification of the chitosan (CS) (95% acetylation, *M_w* = 450 *kDa*; Yuhuan Marine Biochemistry Co., Ltd, Zhejiang, China). The cyclo(RGDfK) peptide (cRGD) was synthesized by ChinaPeptides Co., Ltd. (Shanghai, China). $\text{NH}_2\text{-PEG-NH}_2$ (PEG₂₀₀₀) and 2, 4,

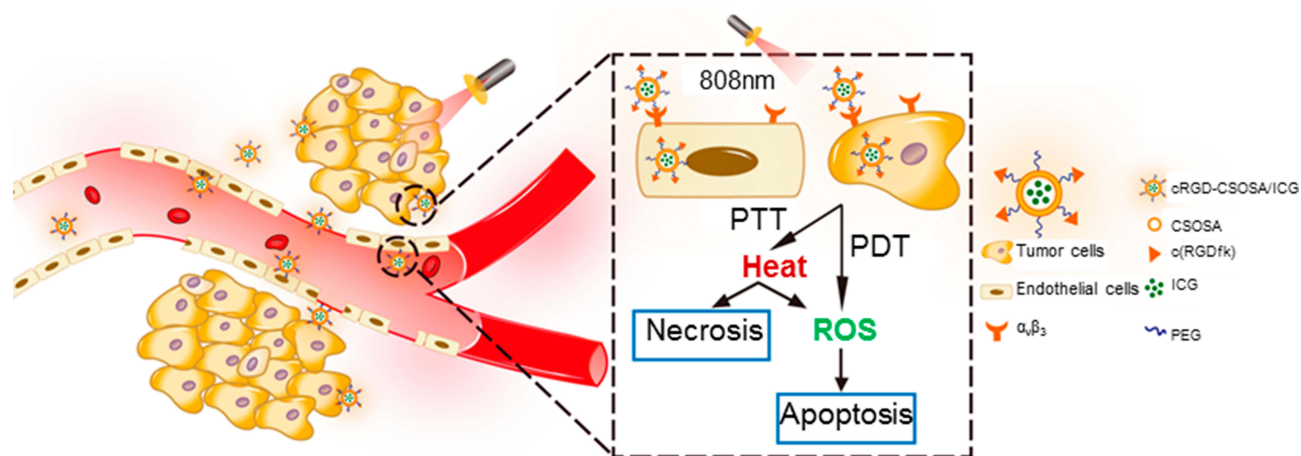


Figure 1 Schematic diagram of phototherapy effect with dual-targeting drug delivery system. The cRGD-CSOSA/ICG nanoparticles are absorbed by tumor cells and neovascular endothelial cells rapidly, and PDT/PTT double efficacy occurs with NIR irradiation to induce cell apoptosis and necrosis for GBM therapy.

6-trinitrobenzene sulfonic acid (TNBS) were purchased from Sigma-Aldrich (Diegem, Belgium). Indocyanine green (ICG), tetrabutylammonium iodide (TBAI), N-hydroxysuccinimide (NHS), pyrene and Rhodamine B isothiocyanate (RBITC) were purchased from Aladdin Reagent Co., Ltd. (Shanghai, China). Stearic acid (SA) was supplied by Shanghai Chemical Reagent Co., Ltd. (Shanghai, China). 1-Ethyl-3-(3-dimethylaminopropyl) carbodiimide hydrochloride (EDC) was purchased from Shanghai Medpep Co, Ltd. N,N'-disuccinimidyl carbonate (DSC) was obtained from Bio Basic Inc., (Toronto, Canada). Methylthiazolotetrazolium (MTT) was obtained from Sigma Chemical Co. Trypsin, Roswell Park Memorial Institute 1640 medium (RPMI-1640) and α -minimum essential medium (α -MEM) were purchased from Gibco (Merelbeke, Belgium). Fetal bovine serum was purchased from Sijiqing Biology Engineering Materials Co, Ltd. All the other chemicals were of analytical or chromatographic grade.

Cell Cultures

The U87 MG cells and HUVECs were purchased from the Cell Bank of Shanghai Institute of Biochemistry and Cell Biology, Chinese Academy of Sciences (Shanghai, China).

The U87 MG cells were cultured at 37 °C in a humidified atmosphere containing 5% CO₂ in α -MEM supplemented with 10% fetal bovine serum and 100 IU/mL penicillin-streptomycin. The HUVECs were cultured in RPMI 1640 medium supplemented with 10% fetal bovine serum (FBS) and 100 IU/mL penicillin-streptomycin. The cells were regularly subcultured using trypsin/ethylene diamine tetraacetic acid (EDTA).

Synthesis and Characteristics of cRGD-Modified Glycolipid-Like Micelles

The glycolipid conjugate CSOSA was synthesized by a previously described method.³⁷ To synthesis cRGD-modified glycolipid-like micelles (cRGD-CSOSA), NH₂-PEG₂₀₀₀-NH₂ was used to connect the cRGD and CSOSA. Briefly, 33 mg PEG₂₀₀₀ and 8 mg DSC were dissolved in dried DMSO, and the mixture was stirred at room temperature for 9 h. Then, 10 mg cRGD was dissolved in dried DMSO, added into the previous mixture dropwise, and stirred for another 9 h. After that, 83 mg of CSOSA was dissolved in 20 mL of deionized (DI) water, and the above mixture was added dropwise and stirred for another 24 h. The final production was dialyzed against DI water for 48 h and then collected by lyophilization.

To verify the chemical structure of CSOSA and cRGD-CSOSA, ¹H-NMR spectroscopy of the chemicals was performed by a ¹H NMR spectrometer (AC-80, Bruker Biospin, Germany). These chemicals were dissolved in D₂O at a concentration of 10 mg/mL. The amino-substitution degrees (SD%) of CSOSA and cRGD-CSOSA were determined by the TNBS test.³⁸ Pyrene was used as a probe to estimate the critical micelle concentrations (CMC).³⁹ A Zetasizer (3000HS, Malvern Instruments Ltd, UK) was used to determine the sizes and zeta potentials of micelles.

Preparation and Characterization of ICG-Loaded Nanoparticles

Hydrophobic indocyanine green (ICG) was obtained by the electrostatic interaction of indocyanine green and prescription dose tetrabutylammonium iodide in DMSO

(ICG:TBAI = 1:2, mol/mol), and the mixture was stirred at room temperature for 30 min. ICG-loaded cRGD-modified glycolipid-like nanoparticles (cRGD-CSOSA/ICG) were prepared by dialysis as in our previous study.⁴⁰ Briefly, hydrophobic ICG (5 mg/mL in DMSO) was added into a CSOSA or cRGD-CSOSA solution (2 mg/mL in deionized water). Then the mixture was stirred at room temperature for 2 h in the dark. After that, the solution was dialyzed against DI water for 24 h and then centrifuged at 8000 rpm for 10 min to remove the unloaded ICG. The size and zeta potential of the ICG-loaded nanoparticles were obtained by the same methods as described above. The morphology of the micelle samples was observed by transmission electron microscopy (TEM, JEM-1230, JEOL). Then, the amount of encapsulated ICG in the micelles was detected by an ultraviolet-visible spectrophotometer (TU-1800PC; Beijing, China) at 784 nm wavelength. The formulas for entrapment efficiency (EE%) and drug loading (DL%) were as follows:

$$EE\% = [\text{weight of ICG in micelles} / \text{weight of ICG in feed}] \times 100\%$$

$$DL\% = [\text{weight of ICG in micelles} / \text{weight of ICG-loaded nanoparticles}] \times 100\%$$

The stability of the ICG-loaded nanoparticles was further investigated using the same method. In brief, ICG, CSOSA/ICG and cRGD-CSOSA/ICG were diluted with DI water to the same concentration and stored at room temperature with light. At a certain time, the UV absorption of the samples was then determined.

Photothermal Conversion Efficiency

The photothermal conversion efficiency was detected by a sensitive thermometer. ICG, CSOSA/ICG and cRGD-CSOSA/ICG with the same ICG concentration were irradiated by a near-infrared laser at 808 nm wavelength, and the temperature of the samples was detected at the setting time point.

In vitro ROS Detection

1,3-Diphenylisobenzofuran (DPBF) is a ROS detection probe.⁴¹ The ICG, CSOSA/ICG and cRGD-CSOSA/ICG solutions were incubated with equal amounts of DPBF and irradiated by a laser. Then, a UV spectrophotometer was used to detect the reduction in the UV absorption of the samples at the maximum absorption wavelength (at 420 nm). The

degree of UV absorption reduction indirectly represent the amount of ROS production.

Singlet oxygen sensor green (SOSG) is a new fluorescent probe that detects intracellular ROS generation.⁴² Briefly, the U87 MG cells (5×10^4) were seeded into culture plates. After 24 h of incubation with 5% CO₂ at 37 °C, they were treated with ICG, CSOSA/ICG, cRGD-CSOSA/ICG and PBS and cultured for 8 h. The medium was then discarded and replaced with fresh α -MEM, and the cells were treated with or without NIR irradiation (2 W/cm², 3 min). After 12 h of incubation, SOSG was added and fluorescence was observed by confocal laser scanning microscopy (CLSM) (Ix81-FV1000, Olympus Co.).

The Expression of Integrin $\alpha_v\beta_3$ on U87 MG Cells and HUVECs

A Western blot assay was used to determine the expression of integrin $\alpha_v\beta_3$ on the U87 MG cells and HUVECs. The U87 MG cells and HUVECs were digested by trypsin and collected. After adding the appropriate RIPA lysis solution, the samples were lysed in an ice bath for 30 min and centrifuged at 8000 rpm for 15 min at 4 °C. The supernatant was collected, and the total cell protein content was obtained by BCA assay. Lastly, the samples were heated for 10 min at 100 °C, and the expression of integrin $\alpha_v\beta_3$ was determined.

Double-Targeting

The U87 MG cells or HUVECs were seeded at a density of 5×10^4 cells/well in 24-well culture plates and cultured for 12 h with 5% CO₂ at 37 °C. Both RBITC-labeled CSOSA and cRGD-CSOSA with the same concentration (100 μ g/mL) were added into 24-well culture plates for 1 h and 4 h at 37 °C, and then CLSM was used to observe the fluorescence of the cells.

Competitive uptake of the U87 MG cells or HUVECs was monitored to examine the internalization pathways of cRGD-modified glycolipid-like micelles. The U87 MG cells or HUVECs were seeded at a density of 5×10^4 cells/well in 24-well culture plates and cultured for 12 h with 5% CO₂ at 37 °C. Solutions of cRGD with concentrations of 0 μ M, 1 μ M, 10 μ M and 20 μ M were added into 24-well culture plates. After 2 h, RBITC-labeled cRGD-CSOSA at the same concentration of 100 μ g/mL was added into 24-well culture plates for 2 h at 37 °C. The fluorescence of the cells was obtained by CLSM.

Cytotoxicity

The U87 MG cells were seeded at a density of 6×10^3 cells/well in 96-well culture plates and cultured for 24 h with 5% CO₂ at 37 °C. ICG, CSOSA/ICG and cRGD-CSOSA/ICG with a series of ICG concentrations were added. The blank culture medium was treated as a blank control. After 8 h, the culture medium was discarded and replaced with fresh α -MEM and then treated with or without NIR irradiation (2 W/cm², 3 min). After 48 h, 20.0 μ L of the MTT solution (5.0 mg/mL) was added and incubated for another 4 h. Then, the medium was discarded and replaced by 200 μ L of DMSO to dissolve the purple formazan crystals. The absorbance of each well at 570 nm was measured by a microplate reader (Bio-Rad, Model 680, USA). Cell viability was calculated based on the cells incubated with the culture medium alone. The cell viability of U87 MG cells in the blank CSOSA or cRGD-CSOSA group was determined by the same method.

In vitro Anti-Angiogenesis

Same process with above. Cytotoxicity of HUVECs exactly same as U87 cells apart from α -MEM was replaced by RPMI 1640.

The HUVECs were seeded at a density of 2×10^5 cells/well in 6-well culture plates and cultured for 24 h with 5% CO₂ at 37 °C. The cells were incubated with ICG, CSOSA/ICG and cRGD-CSOSA/ICG of the same concentrations (10 μ g/mL). The blank culture medium was treated as a blank control. After 8 h, we discarded the culture medium and the HUVECs were digested with trypsin and seeded at a density of 5×10^4 cells/well in 96-well culture plates coated with Matrigel matrix. Then, the HUVECs were treated with or without NIR irradiation (2 W/cm², 3 min). The cells were then cultured for 6 h, and optical microscopy was used to observe the formation of the cavities in each group.

In vivo Imaging and Biodistribution of cRGD-CSOSA in Tumor-Bearing Model

To prepare the xenograft tumor mouse model, a suspension of approximately 1.0×10^7 U87 MG cells was inoculated subcutaneously in nude mice (6–8 weeks). All the studies were approved by the Ethical Committee of Zhejiang University and were conducted in accordance with the national regulations and protocols.

When the tumor size reached approximately 150 mm³, ICG (1 mg/kg), CSOSA/ICG (1 mg/kg) or cRGD-CSOSA/ICG (1 mg/kg) was injected via the tail vein to investigate the tumor fluorescence imaging. At the setting time point after injection, the mice were observed by the Maestro in vivo imaging system (CRI Inc.). The fluorescence images of the excised organs and tumor tissues were also obtained by IVIS spectroscopy.

To observe the distribution of cRGD-CSOSA in the tumor tissue, RBITC-labeled CSOSA (5 mg/kg) or cRGD-CSOSA (5 mg/kg) was injected via the tail vein when the tumor size reached approximately 150 mm³. After 24 h, all the mice in the different groups were euthanized. The excised tumors were frozen and cut into 5 μ m slices for immunofluorescence staining to detect CD31. The fluorescence distribution of tumor tissues was obtained by CLSM.

To investigate the effect of dual-targeted phototherapy on the cRGD-CSOSA targeting distribution in tumor tissue, when the tumor size reached approximately 150 mm³, the xenografted tumor-bearing mice were randomly divided into four groups: CSOSA/ICG (3 mg/kg) with NIR irradiation; cRGD-CSOSA/ICG (3 mg/kg) with NIR irradiation; CSOSA/ICG (3 mg/kg); cRGD-CSOSA/ICG (3 mg/kg). Various formulations were injected via the tail vein. After 24 h, the tumors of the xenografted tumor mice in the first two groups were treated with NIR irradiation (1 W/cm², 3 min). The last two groups without NIR irradiation were used as negative controls. After 24 h, xenografted tumor mice in the CSOSA/ICG with NIR irradiation and CSOSA/ICG groups were treated with RBITC-labeled CSOSA (5 mg/kg). Mice in cRGD-CSOSA/ICG with or without NIR irradiation groups were treated with RBITC-labeled cRGD-CSOSA (5 mg/kg). Twenty-four hours later, all the mice in the different groups were euthanized. The excised tumors were frozen and cut into 5 μ m slices, and the fluorescence distribution of the tumor tissues was obtained by CLSM.

In vivo Phototherapy

When the tumor size reached approximately 150 mm³, saline, ICG, CSOSA/ICG or cRGD-CSOSA/ICG with a dose of 3 mg ICG/kg was injected via the tail vein. After 24 h, the tumors of xenografted tumor mice were treated with NIR irradiation (1 W/cm², 5 min), and a temperature-sensitive camera was used to record temperature changes in the mice.

When the tumor size reached approximately 120 mm³, the xenografted tumor-bearing mice were randomly divided into eight groups (n=5): ICG (3 mg/kg) with NIR irradiation,

CSOSA/ICG (3 mg/kg) with NIR irradiation, cRGD-CSOSA/ICG (3 mg/kg) with NIR irradiation, saline with NIR irradiation, ICG (3 mg/kg), CSOSA/ICG (3 mg/kg), cRGD-CSOSA/ICG (3 mg/kg) and saline. Various formulations were injected via the tail vein. After 24 h, the tumors of the xenografted tumor mice in the first four groups were treated with NIR irradiation (1 W/cm^2 , 3 min); the last four groups that were treated without NIR irradiation were used as negative controls. Five injections and NIR irradiations were administered every other day for the first 10 days. The antitumor activity was evaluated according to the tumor volume at different times post-administration, and the tumor volumes and mouse weights were measured every two days after the first injection.

All the mice in the different groups were euthanized 21 days post-administration. The excised tumors and major organs (heart, liver, spleen, lung, and kidney) were fixed in formalin and cut into $5 \mu\text{m}$ slices for hematoxylin and eosin (H&E) staining. In addition, immunohistochemistry (IHC) analyses were carried out using monoclonal antibodies against CD31, Ki67 and C-caspase3.

Statistical Analysis

All data are expressed as the mean value \pm standard deviation (SD) of three independent measurements. Statistical analysis was performed using one-way ANOVA or Student's *t*-test. *P*-values < 0.05 were regarded as statistically significant.

Results and Discussion

Preparation and Characterization of cRGD-CSOSA Micelles

First, glycolipid-like polymers CSOSA were obtained by the reaction between the amino groups of CSO and the carboxyl group of SA in the presence of EDC. Then, cRGD-CSOSA was obtained by two-step amide reactions using DSC as the bridge chain to connect c(RGDfk), $\text{H}_2\text{N-PEG}_{2000}\text{-NH}_2$, and CSOSA (Figure S1). The final production was collected by lyophilization. The $^1\text{H-NMR}$ spectrum in D_2O showed the structure of cRGD-CSOSA (Figure 2A). The peaks at 1.09 ppm and 1.12 ppm belonged to the methylene hydrogen and methyl hydrogen of SA, respectively. The intense peaks between 3.4 ppm and 3.6 ppm belonged to the methylene hydrogen of $\text{NH}_2\text{-PEG}_{2000}\text{-NH}_2$. The tiny peaks between 7.0 ppm and 7.2 ppm belonged to the amino acids of benzene from cRGD. The results indicated that cRGD had been successfully

conjugated to CSOSA. This was further verified by amino-substitution degrees (SD%) of CSOSA and cRGD-CSOSA which were 10.3% and 13.7%, respectively.

The synthesized CSOSA and cRGD-CSOSA were easy to self-assemble into nanosized micelles in aqueous solution. Figure 2B shows the variation of the I_1/I_3 ratio against the logarithmic concentration (Lg C) of CSOSA and cRGD-CSOSA. The corresponding concentrations of the turning points indicated the critical micelle concentration (CMC) values of CSOSA and cRGD-CSOSA, which were $57.5 \mu\text{g/mL}$ and $69.8 \mu\text{g/mL}$, respectively.

The average particle size of cRGD-CSOSA was $93.5 \pm 1.4 \text{ nm}$, which was slightly higher than that of CSOSA, determined as $64.3 \pm 1.6 \text{ nm}$ (Table S1). The zeta potentials of cRGD-CSOSA and CSOSA were determined to be $28.3 \pm 0.9 \text{ mV}$ and $32.5 \pm 0.2 \text{ mV}$ (Table S1), respectively. These results might be attributed to the modification of hydrophilic PEG chains and cRGD on the surface of CSOSA.

Preparation and Characterization of ICG-Loaded Nanoparticles

ICG was selected as a model photosensitizer. The average particle sizes of CSOSA/ICG and cRGD-CSOSA/ICG were $113 \pm 5.3 \text{ nm}$ and $127 \pm 10.8 \text{ nm}$, respectively, which were slightly higher than those of their blank micelles (Table S1). The reason for this difference might be that the structure of the nanoparticles was enlarged as ICG entered the hydrophobic core. The zeta potentials of CSOSA/ICG and cRGD-CSOSA/ICG were measured as $28.5 \pm 0.5 \text{ mV}$ and $25.0 \pm 0.9 \text{ mV}$ (Table S1), respectively. The TEM images show that the CSOSA/ICG and cRGD-CSOSA/ICG nanoparticles were spherical (Figure 2C and D). The EE% and DL % of cRGD-CSOSA/ICG were determined as $64.85 \pm 9.97\%$ and $6.09 \pm 0.88\%$, respectively, which were slightly lower than those of CSOSA/ICG (measured as $76.84 \pm 5.88\%$ and $7.14 \pm 0.51\%$, respectively) (Table S1, Figure S2 and S3). The hydrophilic PEG chains and cRGD modified on the surface of CSOSA might lead to a slight decrease in the EE% and DL % values due to a decrease in the hydrophobic force in the micellar hydrophobic core.⁴³

As reported, ICG is extremely unstable in aqueous solution, because it is prone to self-aggregation in water, and its degradation is accelerated with light. The UV absorption of ICG decreased significantly within a week, suggesting that ICG might have been denatured. In comparison, there were no obvious changes in the UV absorption of either the CSOSA/ICG or cRGD-CSOSA/ICG

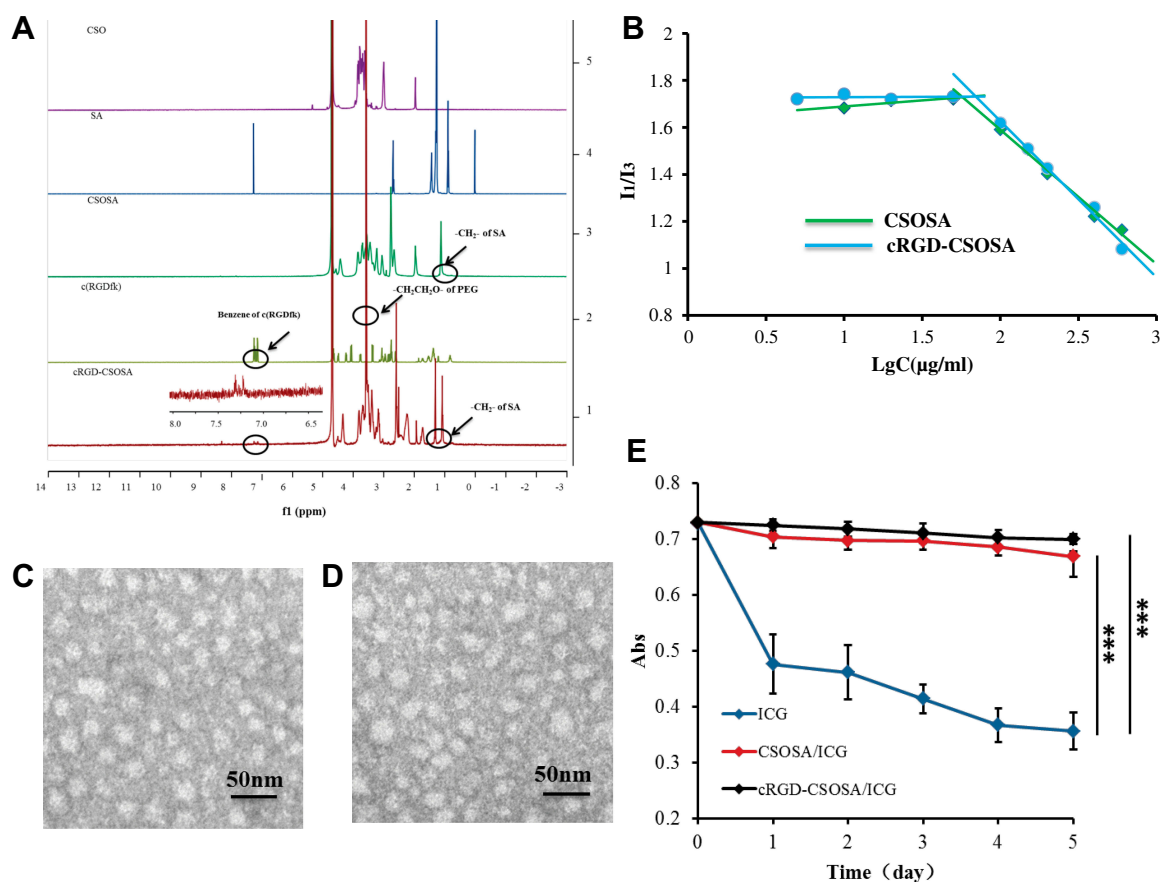


Figure 2 Characterization of cRGD-CSOSA. (A) $^1\text{H-NMR}$ spectra of CSO, SA, CSOSA, cRGD, and cRGD-CSOSA in D_2O . (B) CMC values of CSOSA and cRGD-CSOSA. (C) TEM images of CSOSA/ICG. (D) TEM images of cRGD-CSOSA/ICG. (E) The stability of ICG-loaded nanoparticles. *** $p < 0.001$.

nanoparticles (Figure 2E). The results indicated that glycolipid-like micelles could improve the stability of ICG.

In vitro Photothermal Conversion Efficiency and ROS Detection

ICG could induce the PTT effect, and the temperatures of ICG, CSOSA/ICG and cRGD-CSOSA/ICG were increased with continuous NIR irradiation (2 W/cm^2 , 3 min) to 46.0°C , 44.4°C and 45.8°C respectively. Compared with PBS, which was increased to 30.5°C , there was a significant difference (Figure 3A). The results indicated that ICG loaded into glycolipid-like micelles exhibited a negligible effect on the ICG photothermal conversion efficiency.

With NIR irradiation, ICG could also promote the production of ROS. Figure 3B shows the decrease in DPBF UV absorption at 420 nm wavelength, which presented the relative amount of ROS after different preparations were treated with NIR irradiation for 3 min, 5 min, and 10 min. The results indicated that the ROS production of CSOSA/ICG and cRGD-CSOSA/ICG was higher than that of ICG. This

difference might be due to the instability in aqueous solution and the accelerated degradation with irradiation of ICG.

The intracellular ROS production mediated by NIR irradiation was also investigated in the U87 MG cells (Figure 3C and D). The intensity of green fluorescence represented the amount of intracellular ROS. The cRGD-CSOSA/ICG with NIR irradiation induced a stronger production of ROS in the cells than did the equivalent of ICG and CSOSA/ICG. Additionally, NIR irradiation alone or formulations without NIR irradiation produced little intracellular ROS. This result might be because glycolipid-like polymeric micelles improved the stability of ICG and cRGD modification enhanced the uptake by cells.

The Expression of Integrin $\alpha_v\beta_3$ on U87 MG Cells and HUVECs

A Western blot assay was used to determine the expression of integrin $\alpha_v\beta_3$ on the HUVECs and U87 MG cells. The results are shown in Figure S4. Both the U87 MG cells and HUVECs highly expressed integrin $\alpha_v\beta_3$. This finding

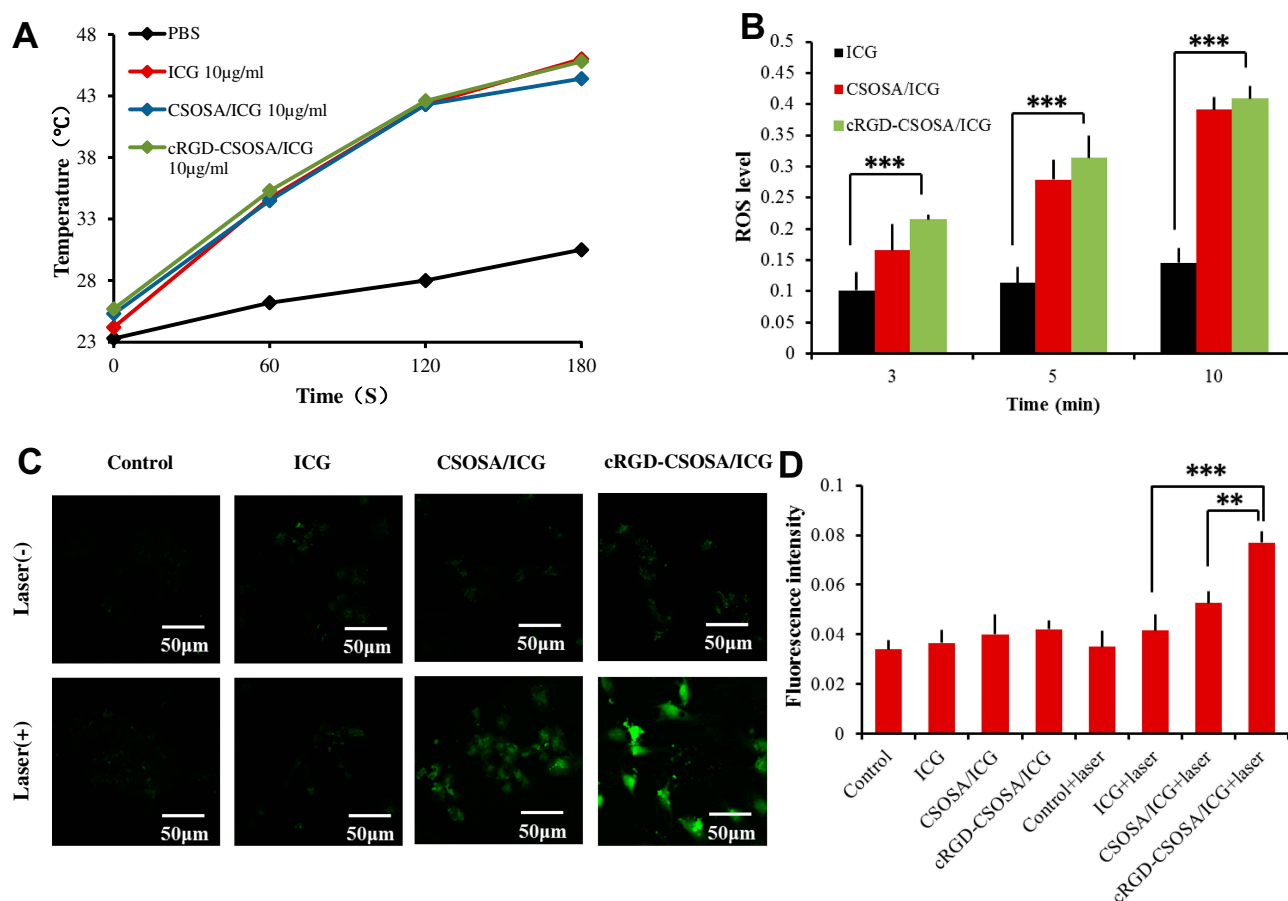


Figure 3 Photothermal conversion efficiency and ROS detection in vitro (A) Photothermal conversion efficiency of ICG, CSOSA/ICG and cRGD-CSOSA/ICG with the NIR irradiation (2 W/cm^2). (B) The production of extracellular ROS by NIR irradiation (2 W/cm^2). (C) The production of intracellular ROS mediated by NIR irradiation (2 W/cm^2 , 3 min). (D) The median fluorescence intensity of intracellular ROS produced by U87 MG cells. ** $p < 0.01$, *** $p < 0.001$.

suggested that the nanoparticles modified by cRGD have the feasibility to target both neovascular endothelial cells and tumor cells.

Cellular Targeting Uptake of cRGD-CSOSA Micelles

RBITC-labeled CSOSA and cRGD-CSOSA were used to determine dual-targeting capability. The intensity of red fluorescence represented the amount of micelle uptake by the cells. The confocal images shown in Figure 4A and B indicate that with the modification of cRGD, the uptake of cRGD-CSOSA in the HUVECs and U87 MG cells significantly increased. As shown in Figure 4C and D, the fluorescence signal in U87 MG cells and HUVECs of the cRGD-CSOSA group was stronger than that in the CSOSA group. To further investigate the internalization mechanism of cRGD-CSOSA, cRGD was used to block integrin $\alpha_v\beta_3$ on the membranes of the HUVECs and U87 MG cells. The results in Figure 5A and B show that after treatment with

increasing concentrations of cRGD, the uptake of cRGD-CSOSA by U87 MG cells and HUVECs decreased gradually. These results suggested that cRGD-CSOSA internalization into the cells was mediated by integrin $\alpha_v\beta_3$ signaling pathways and that cRGD modification could enhance the uptake of micelles by U87 MG cells and HUVECs. This result indicated that cRGD-CSOSA is a potential dual-targeting carrier that could target both tumor cells and neovascular endothelial cells.

Cytotoxicity Assay

An MTT assay was used to determine in vitro cytotoxicity. As shown in Figure 6A, cRGD-CSOSA/ICG and CSOSA/ICG showed excellent cytotoxicity in the presence of NIR irradiation. When the ICG concentration was $5 \mu\text{g/mL}$, cRGD-CSOSA/ICG and CSOSA/ICG caused approximately 52.9% and 34.5% cell death, respectively, with NIR irradiation. When the ICG concentration was $10 \mu\text{g/mL}$, cRGD-CSOSA/ICG and

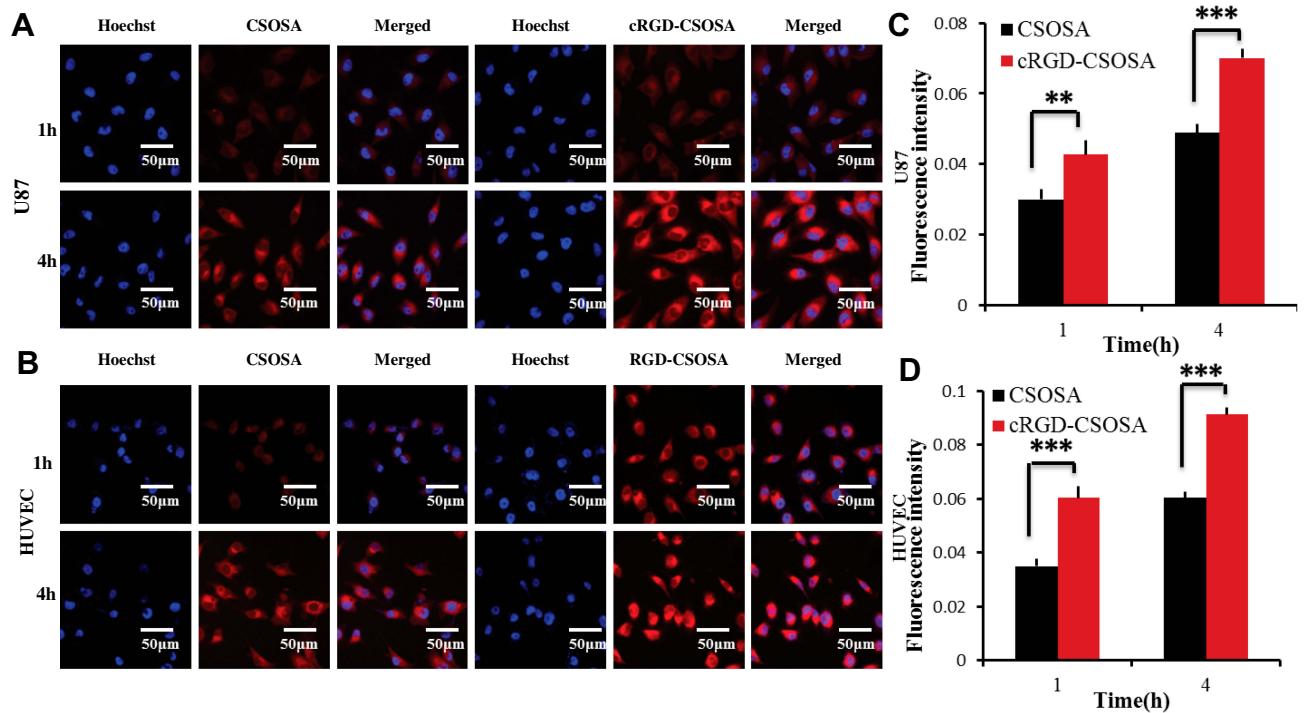


Figure 4 Dual-targeting uptake of cRGD-CSOSA. U87 MG cells (A) and HUVECs (B) were incubated with CSOSA and cRGD-CSOSA for 1 and 4 h, respectively. (C) The median fluorescence intensity of U87 MG cells were incubated with different micelles for 1 and 4 h, respectively. (D) The median fluorescence intensity of HUVECs were incubated with different micelles for 1 and 4 h, respectively. (Data are represented as mean \pm SD, n=3). **p < 0.01, ***p < 0.001.

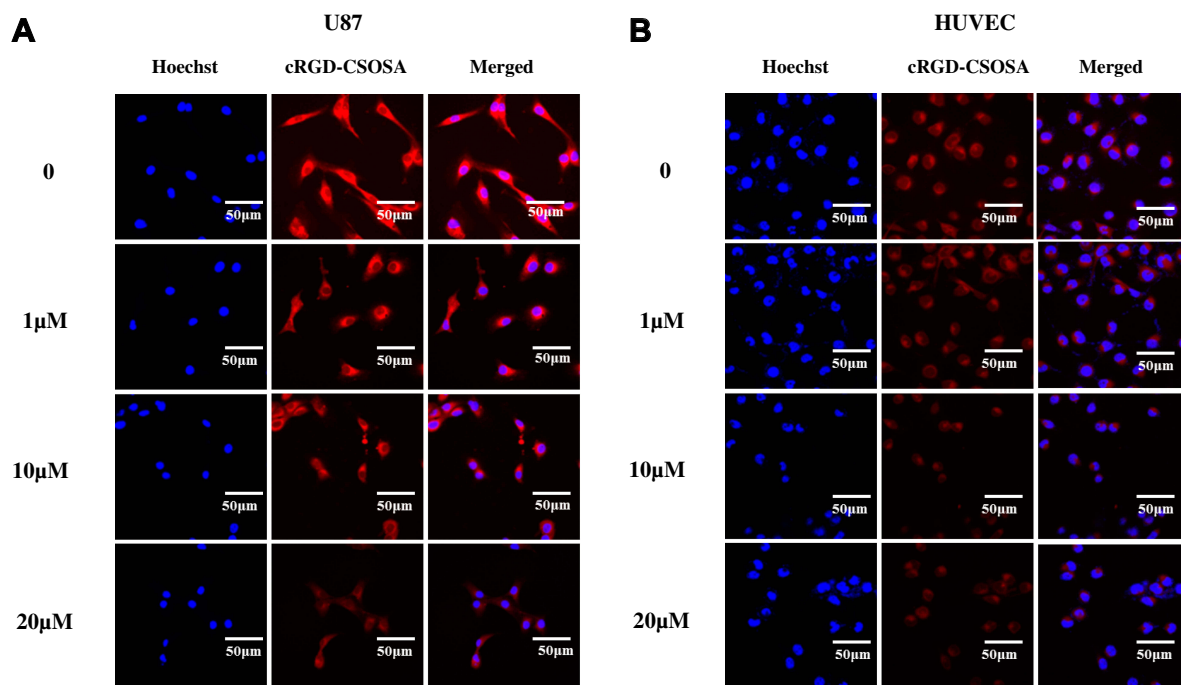


Figure 5 The internalization mechanism of cRGD-CSOSA, after incubation with cRGD at 0 μ M, 1 μ M, 10 μ M, 20 μ M for 2 h, U87 MG cells (A) and HUVECs (B) were incubated with cRGD-CSOSA for 2 h.

CSOSA/ICG caused approximately 76.2% and 69.9% cell death, respectively. In general, cRGD-CSOSA/ICG exhibited higher cytotoxicity to cells than did CSOSA/

ICG, which was mainly due to the high affinity of cRGD with the integrin $\alpha_v\beta_3$ on the membrane of U87 MG cells. In comparison, ICG had little cytotoxicity with

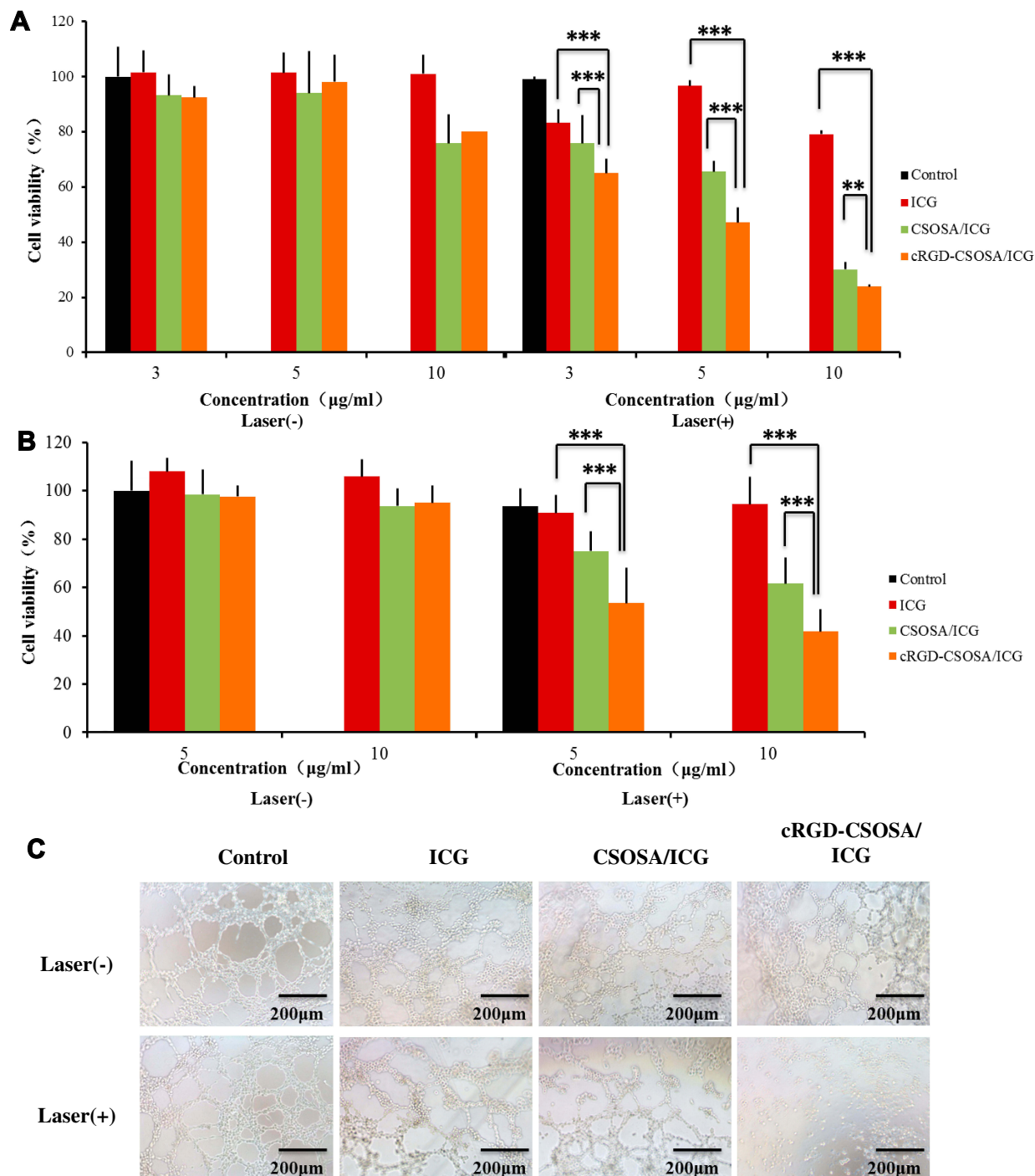


Figure 6 In vitro cytotoxicity and anti-angiogenesis. **(A)** In vitro cytotoxicity of ICG, CSOSA/ICG and cRGD-CSOSA/ICG with the NIR irradiation (2 W/cm², 3 min). **(B)** The effects of ICG-loaded nanoparticles on proliferation of HUVECs with the NIR irradiation (2 W/cm², 3 min). **(C)** The ability of ICG-loaded nanoparticles to anti-angiogenesis with the NIR irradiation (2 W/cm², 3 min). **p < 0.01, ***p < 0.001.

NIR irradiation, possibly due to its poor stability and internalization by cells. Moreover, the ICG and ICG-loaded nanoparticles showed insignificant cytotoxicity without NIR irradiation. In addition, as shown in

[Figure S5](#), the cell survival rate of both the CSOSA and cRGD-CSOSA treated groups was approximately 80%, even at a concentration of 200 µg/mL. These results suggest that cRGD-CSOSA is a safe nanocarrier.

In vitro Anti-Angiogenesis

The MTT assay was also used to determine the effects of ICG-loaded nanoparticles on the proliferation ability of HUVECs. As shown in [Figure 6B](#), cRGD-CSOSA/ICG and CSOSA/ICG showed significant inhibition of HUVECs proliferation with NIR irradiation. When the concentration of ICG was 5 $\mu\text{g/mL}$, the cell inhibition rate of cRGD-CSOSA/ICG was 46.7% which was higher than that of CSOSA/ICG (25.3%). When the concentration of ICG was 10 $\mu\text{g/mL}$, the inhibition rates of cRGD-CSOSA/ICG and CSOSA/ICG were 58.5% and 38.6%, respectively. However, ICG had little effect on the proliferation of HUVECs in the presence of NIR irradiation. Each preparation exhibited a negligible effect on the proliferation ability of HUVECs without NIR irradiation. These results suggested that cRGD-CSOSA/ICG could be used to inhibit the proliferation of HUVECs following NIR irradiation.

The angiogenesis assay was used to further investigate the ability of ICG, CSOSA/ICG and cRGD-CSOSA/ICG nanoparticles to produce an anti-angiogenic effect. The optical microscopy images in [Figure 6C](#) show that the tube-like structures in the cRGD-CSOSA/ICG group with NIR irradiation were destroyed, and the HUVECs were scattered. The tube-like structures in the CSOSA/ICG group with NIR irradiation were partially damaged. However, the ICG with NIR irradiation groups formed tube-like structures. Additionally, the HUVECs in each group could spontaneously form a tube-like structure without NIR irradiation. The results indicated that cRGD-CSOSA/ICG-mediated phototherapy could overcome the proliferation of neovascular endothelial cells and block angiogenesis with NIR irradiation.

In vivo Imaging and Biodistribution

ICG could be used as a fluorescence probe for tumor imaging because of the fluorescence production in the presence of NIR irradiation with a wavelength of 790 nm. Integrin $\alpha_v\beta_3$ is highly expressed on the tumor cells and neovascular endothelial cells, which could contribute to the ability of cRGD peptides to target tumor tissues, as well as to tumor diagnosis. As shown in [Figure 7A](#), compared with CSOSA/ICG and ICG, a large number of cRGD-CSOSA/ICG nanoparticles accumulated at tumor sites 12 h post-administration. The distribution of cRGD-CSOSA/ICG in the tumors increased over time with no obvious discrepancy until 72 h, while the fluorescence signal of ICG and CSOSA/ICG in the tumors

was weakened after 48 h. In addition, only some of the CSOSA/ICG nanoparticles accumulated in the tumor tissue by the enhanced permeability and retention (EPR) effect. The tumor tissues and main organs of the nude mice were harvested to investigate the fluorescence imaging ([Figure 7B](#)). No significant fluorescence was found in the major organs of all groups. Additionally, the fluorescence of the cRGD-CSOSA/ICG group in the tumors was significantly stronger than that in the other groups. These results indicated that glycolipid-like micelles modified with cRGD could actively target the tumor and increase the distribution and accumulation of cRGD-CSOSA/ICG in the tumor. In addition, due to the fluorescence of ICG, cRGD-CSOSA/ICG could be used for tumor monitoring and diagnosing.

To further investigate the distribution of CSOSA and cRGD-CSOSA in tumor tissue after dual-targeted phototherapy, fluorescence imaging of tumor tissue sections was obtained by CLSM ([Figure 7C](#)). Green fluorescence was used to label the neovascular endothelial cells, and the intensity of red fluorescence represented the amount of micelle distribution in the tumor tissue. Compared with that of CSOSA, the distribution of cRGD-CSOSA in the neovascular endothelial cells and tumor cells increased significantly. This result indicated that cRGD-CSOSA is a potential dual-targeting carrier that could target both neovascular endothelial cells and tumor cells.

The distribution of cRGD-CSOSA in tumor tissue after was investigated. As shown in [Figure 7D](#), the intensity of red fluorescence represented the amount of micelle distribution in the tumor tissue, and a large number of cRGD-CSOSA micelles accumulated in the tumor tissue after dual-targeted phototherapy. However, there was no significant change in CSOSA accumulation in the tumor tissue after phototherapy. This result suggested that dual-targeted phototherapy with cRGD modified CSOSA micelles could preferentially destroy the tumor vascular structure and further improve drug delivery to tumor cells. This phenomenon might be due to the increased permeability of blood vessels through the formation of endothelial intercellular gaps via endothelial cell microtubule depolymerization following vascular-targeting photodynamic therapy; thus, tumor uptake of nanoparticles was significantly increased.

In vivo Antitumor Activity

The in vivo antitumor efficiency of ICG-loaded nanoparticles with NIR irradiation was investigated on U87 MG tumor-xenografted nude mice. The increased temperature

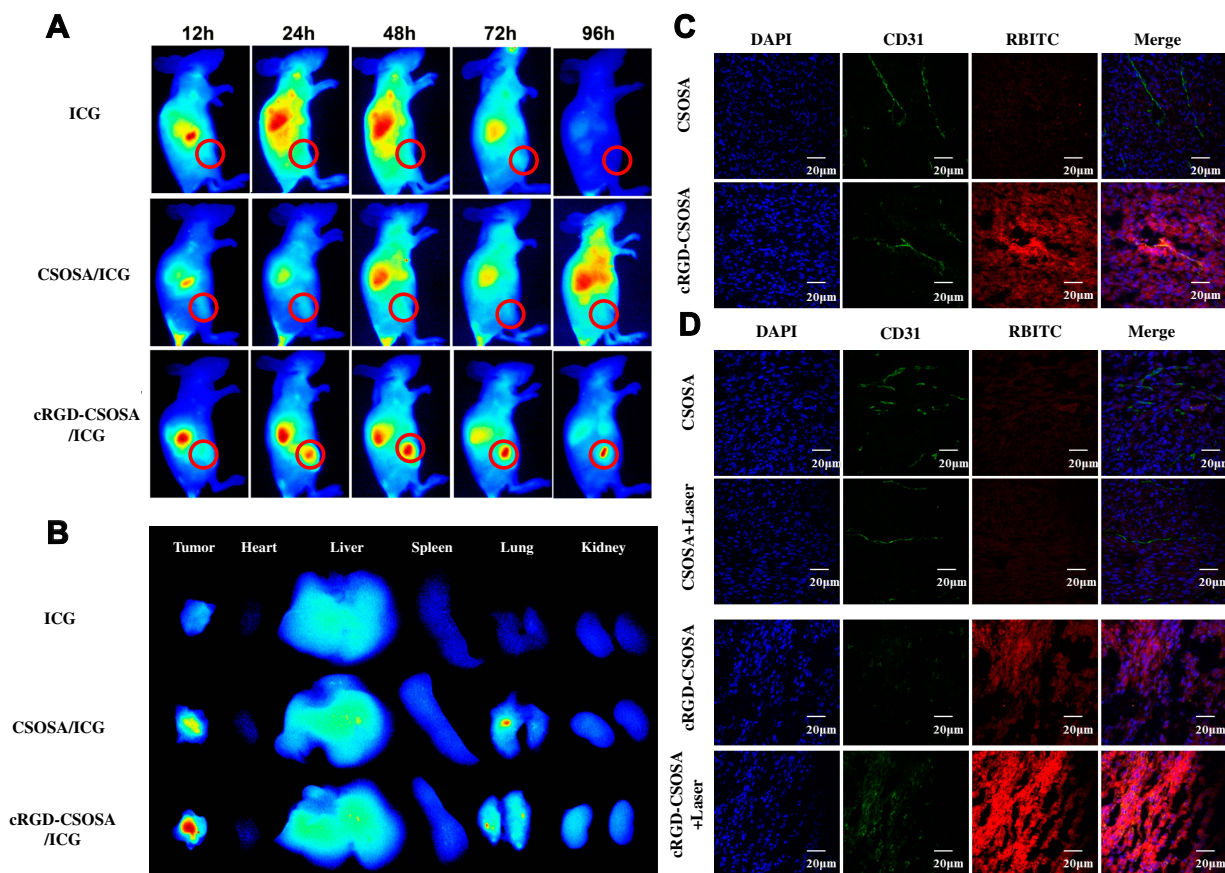


Figure 7 In vivo Imaging and bio-distribution. **(A)** In vivo Imaging and distribution of ICG, CSOSA/ICG and cRGD-CSOSA/ICG after i.v. injection for 12, 24, 48, 72 and 96 h. **(B)** The fluorescent imaging of tumor tissues and main organs. **(C)** The distribution of CSOSA and cRGD-CSOSA in tumor tissue after i.v. injection for 24 h. **(D)** After phototherapy, the distribution of CSOSA and cRGD-CSOSA in tumor tissue.

induced by NIR irradiation was measured by in vivo infrared thermal imaging and analyzed by FLIR QuickReport software (Figure 8A). The intratumoral temperature of the cRGD-CSOSA/ICG group increased to 56.4 °C after NIR irradiation, which was significantly higher than those of the CSOSA/ICG (47.4 °C), free ICG (44.8 °C) and saline (42.3 °C) groups. The reason for this difference was that cRGD modified micelles could enhance the active targeting ability for efficient intratumoral accumulation and cell uptake, and the micellar structure improved the stability of ICG.

The tumor growth curves and ex vivo photograph of U87 MG tumors from each group after 21 days of administration are shown in Figure 8B and Figure S6, respectively. The cRGD-CSOSA/ICG group treated with NIR irradiation showed the highest tumor inhibition. CSOSA/ICG with NIR irradiation exhibited a weaker tumor inhibition compared with that of cRGD-CSOSA/ICG due to the lack of an active targeting effect. The free ICG with NIR irradiation group had negligible therapeutic effects due to

its lack of stability and selectivity. The combined NIR irradiation and drug delivery systems exhibited better anticancer effects than those groups without irradiation. As shown in Figure 8C, each treated group displayed no significant changes in body weight, which was similar to the saline-treated group. These results indicated that cRGD-CSOSA/ICG had good biocompatibility and low systemic toxicity. The final tumor weights are shown in Figure 8D, and the group treated by cRGD-CSOSA/ICG nanoparticles with NIR irradiation (80.00%) displayed the highest tumor-inhibition efficiency, which was higher than that of ICG (9.08%) and CSOSA/ICG (42.42%) with NIR irradiation. Hematoxylin and eosin (H&E) staining also demonstrated that the most serious tumor tissue damage was caused by cRGD-CSOSA/ICG nanoparticles with NIR irradiation (Figure 9B). Tumor sections in saline+laser group showed compact and organized desmoplastic structure. In comparison, wizened, vacuous and irregular cellular morphologies as indicated by black arrows, were observed in CSOSA/ICG+laser and cRGD-CSOSA/ICG+laser groups. The slices

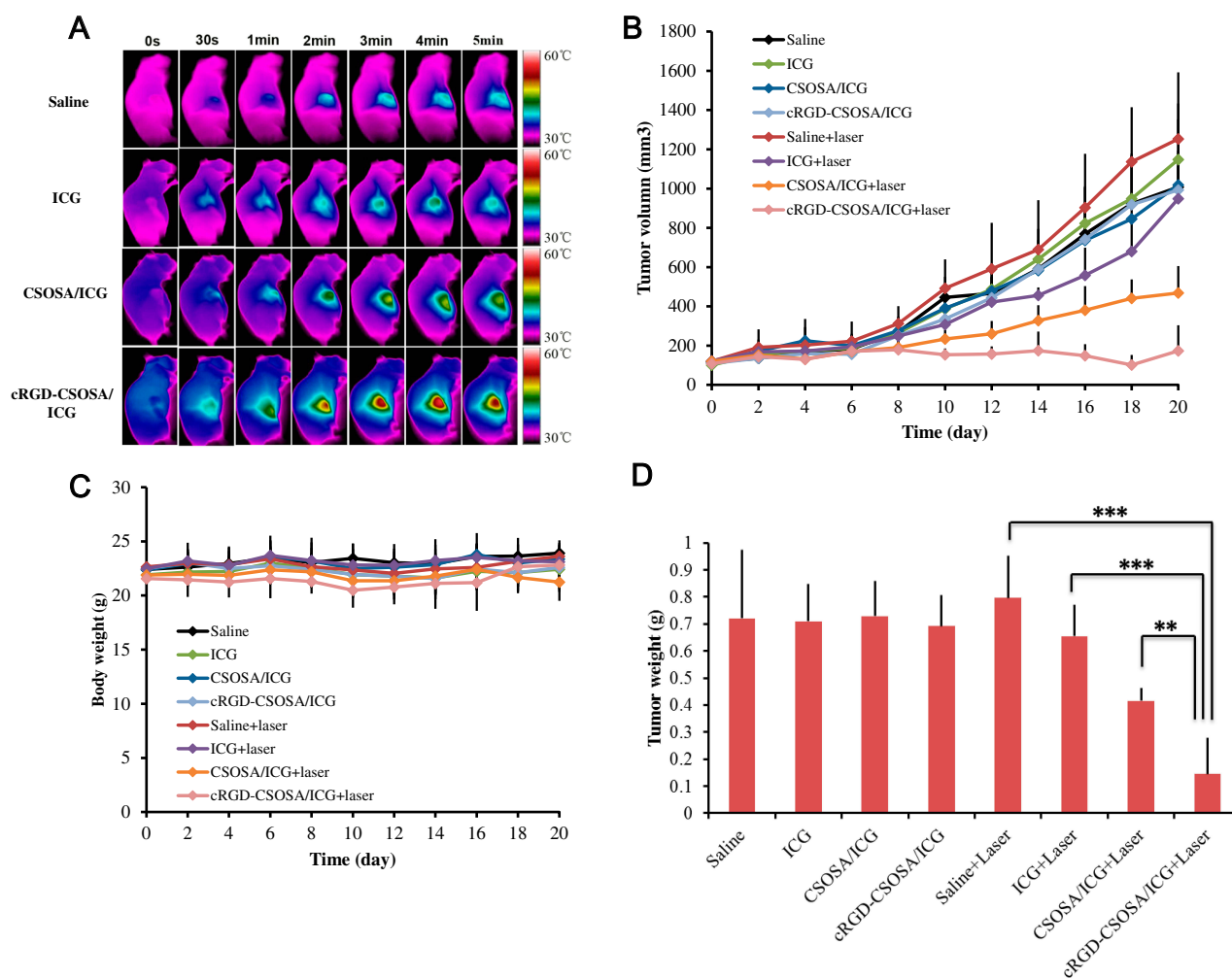


Figure 8 In vivo antitumor activity. **(A)** In vivo infrared thermal imaging of ICG, CSOSA/ICG and cRGD-CSOSA/ICG after i.v. injection for 24 h (1 W/cm²). **(B)** Tumor volume changes (n=5). **(C)** Variations of body weight (n=5). **(D)** Final tumor weights (mean ± SD, n=5), **p < 0.01, ***p < 0.001.

of major organs (heart, liver, spleen, lung, and kidney) (Figure 9A) from mice treated by nanoparticles with NIR irradiation showed no significant abnormalities or lesions compared to those of the saline-treated mice, indicating a lack of appreciable organ damage and further suggesting the low toxicity of the nanoparticles.

To further investigate the anti-angiogenic efficacy of cRGD-CSOSA/ICG with NIR irradiation, immunohistochemical staining analysis was carried out on tissue sections of tumors in all treatment groups. As shown in Figure 9C, the expression of CD31 (brown) in tumor samples treated with cRGD-CSOSA/ICG under NIR irradiation decreased significantly compared with other groups. The results indicated that cRGD-modified nanoparticles could target neovascular endothelial cells to block angiogenesis. Furthermore, to investigate tumor apoptosis in vivo, C-caspase3 staining was conducted (Figure 9D).

The cRGD-CSOSA/ICG with NIR irradiation significantly enhanced the expression of C-caspase3 (brown) in tumor tissues. Ki67 staining was conducted to observe the cell proliferation ability of tumors in vivo. The expression of Ki67 (brown) in tumor tissue treated with cRGD-CSOSA/ICG and NIR irradiation was low (Figure 9E). In comparison, without NIR irradiation, the tumor tissues remained intact, and the expression levels of CD31, C-caspase3 and Ki67 were not different from those of the negative control (Figure S7). These results further demonstrated that dual-targeting cRGD-CSOSA/ICG combined with PTT and PDT could potentially inhibit tumor growth.

Conclusion

In this study, cRGD-CSOSA/ICG nanoparticles were developed for dual-targeting of both neovascular endothelial cells and tumor cells and stabilizing ICG, which

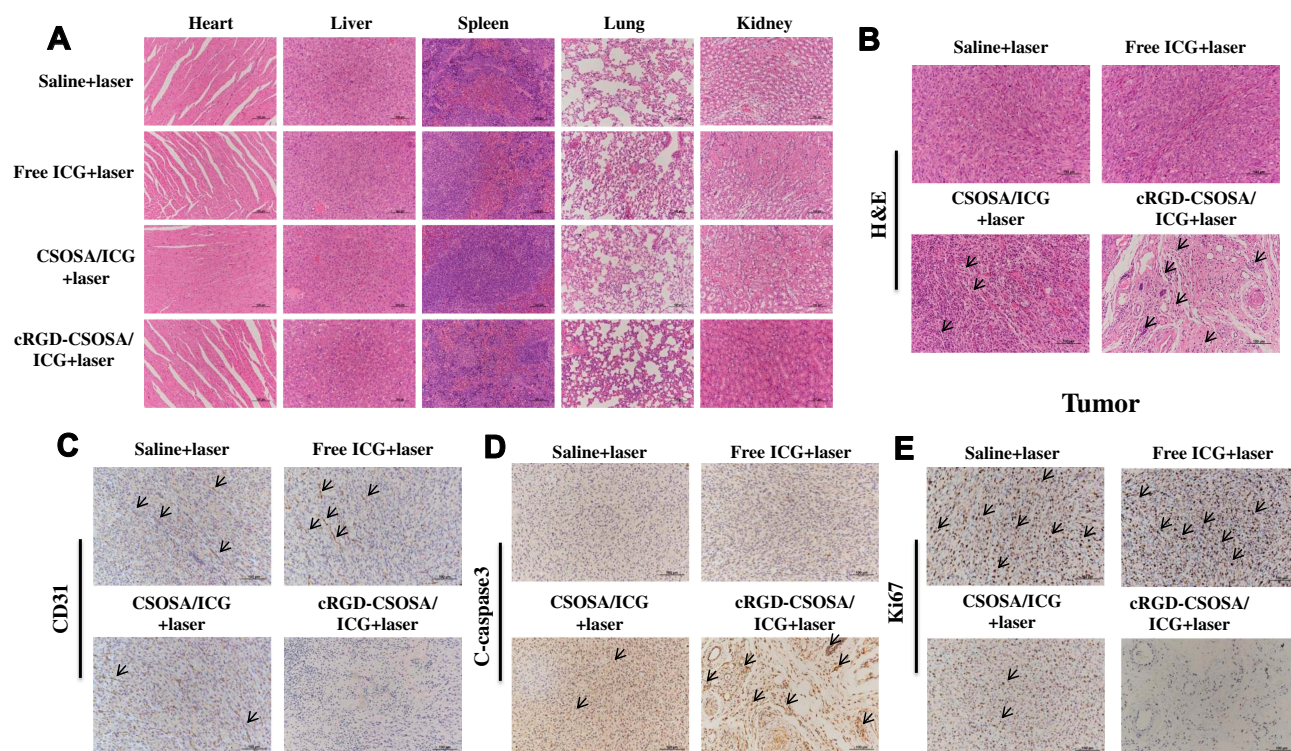


Figure 9 Histological evaluation of U87 MG tumor xenografted nude mice model in four groups with NIR irradiation. **(A)** H&E images of major organs. **(B)** H&E images of tumor tissue. The arrows indicate the apoptotic cells. **(C)** Tumor blood vessel staining with CD 31 antibody (brown). **(D)** The induction of apoptosis in vivo studies on tumor tissues stained with C-Caspase3 antibodies (brown). **(E)** Cell proliferation evaluation by Ki67 staining (brown).

mediates the phototherapy of glioblastoma. Importantly, cRGD-CSOSA/ICG nanoparticles could selectively accumulate in neovascular endothelial cells and tumor cells and mediate PDT and PTT for glioblastoma, resulting in the significant apoptosis of tumor cells and anti-angiogenic effect. Furthermore, cRGD grafted CSOSA as a micelle structure stabilized ICG in vivo. With NIR irradiation, cRGD-CSOSA/ICG nanoparticles stimulated the production of ROS and increased the temperature greatly, which further activated caspase-3 and induced tumor cell apoptosis. In addition, the proliferation of neovascular endothelial cells was inhibited, and the structure of tumor vessels was destroyed, which further enhanced drug delivery and inhibited angiogenesis. Therefore, cRGD-CSOSA/ICG nanoparticles could realize dual-targeting glioblastoma and neovascularization, and further improve glioblastoma treatment efficiency by combining PDT and PTT, representing a potential therapy for the treatment of glioblastoma.

Acknowledgments

We appreciate the financial support from the National Natural Science Foundation of China (NSFC No. 81773648). We

thank Wei Yin (Core Facilities, Zhejiang University School of Medicine) for her assistance with CLSM.

Disclosure

There are no conflicts of interest to declare in this work.

References

- Bonavia R, Inda MD, Cavenee WK, Furnari FB. Heterogeneity maintenance in glioblastoma: a social network. *Cancer Res.* 2011;71(12):4055–4060. doi:10.1158/0008-5472.CAN-11-0153
- Kesharwani SS, Kaur S, Tummala H, Sangamwar AT. Overcoming multiple drug resistance in cancer using polymeric micelles. *Expert Opin Drug Del.* 2018;15(11):1127–1142. doi:10.1080/17425247.2018.1537261
- Liu F, Mischel PS. Targeting epidermal growth factor receptor co-dependent signaling pathways in glioblastoma. *Wiley Interdiscipl Rev.* 2018;10(1):e1398.
- Lu VM, Jue TR, McDonald KL, Rovin RA. The survival effect of repeat surgery at glioblastoma recurrence and its trend: a systematic review and meta-analysis. *World Neurosurg.* 2018;115(453):453–459. e3. doi:10.1016/j.wneu.2018.04.016
- Yamauchi K, Yang M, Hayashi K, et al. Induction of cancer metastasis by cyclophosphamide pretreatment of host mice: an opposite effect of chemotherapy. *Cancer Res.* 2008;68(2):516. doi:10.1158/0008-5472.CAN-07-3063
- Combs SE, Heeger S, Haselmann R, Edler L, Debus J, Schulz-Ertner D. Treatment of primary glioblastoma multiforme with cetuximab, radiotherapy and temozolomide (GERT) – Phase I/II trial: study protocol. *BMC Cancer.* 2006;6(1):1. doi:10.1186/1471-2407-6-133

7. Bryukhovetskiy I, Shevchenko V. Molecular mechanisms of the effect of TGF- β 1 on U87 human glioblastoma cells. *Oncol Lett.* 2016;12(2):1581–1590. doi:10.3892/ol.2016.4756
8. Hu D, Sheng Z, Gao G, et al. Activatable albumin-photosensitizer nanoassemblies for triple-modal imaging and thermal-modulated photodynamic therapy of cancer. *Biomaterials.* 2016;93:10–19. doi:10.1016/j.biomaterials.2016.03.037
9. Sheng Z, Hu D, Zheng M, et al. Smart human serum albumin-indocyanine green nanoparticles generated by programmed assembly for dual-modal imaging-guided cancer synergistic phototherapy. *ACS Nano.* 2014;8(12):12310–12322. doi:10.1021/nn5062386
10. Bisker G, Yeheskel-Hayon D, Minai L, Yelin D. Controlled release of Rituximab from gold nanoparticles for phototherapy of malignant cells. *J Controlled Release.* 2012;162(2):303–309. doi:10.1016/j.jconrel.2012.06.030
11. Keyvan Rad J, Mahdavian AR, Khoei S, Shirvalilou S. Enhanced photogeneration of reactive oxygen species and targeted photothermal therapy of C6 glioma brain cancer cells by folate-conjugated gold-photoactive polymer nanoparticles. *ACS Appl Mater Interfaces.* 2018;10(23):19483–19493. doi:10.1021/acsami.8b05252
12. Dixit S, Miller K, Zhu Y, et al. Dual receptor-targeted theranostic nanoparticles for localized delivery and activation of photodynamic therapy drug in glioblastomas. *Mol Pharm.* 2015;12(9):3250–3260. doi:10.1021/acs.molpharmaceut.5b00216
13. Guo D, Xu S, Wang N, et al. Prodrug-embedded angiogenic vessel-targeting nanoparticle: a positive feedback amplifier in hypoxia-induced chemo-photo therapy. *Biomaterials.* 2017;144:188–198. doi:10.1016/j.biomaterials.2017.08.032
14. Peng C-L, Lin H-C, Chiang W-L, et al. Anti-angiogenic treatment (Bevacizumab) improves the responsiveness of photodynamic therapy in colorectal cancer. *Photodiagnosis Photodyn Ther.* 2018;23:111–118. doi:10.1016/j.pdpdt.2018.06.008
15. Liang Y, Hyder SM. Proliferation of endothelial and tumor epithelial cells by progesterin-induced vascular endothelial growth factor from human breast cancer cells: paracrine and autocrine effects. *Endocrinology.* 2005;146(8):3632–3641. doi:10.1210/en.2005-0103
16. Jhaveri N, Chen TC, Hofman FM. Tumor vasculature and glioma stem cells: contributions to glioma progression. *Cancer Lett.* 2016;380(2):545–551. doi:10.1016/j.canlet.2014.12.028
17. Anderson JC, McFarland BC, Gladson CL. New molecular targets in angiogenic vessels of glioblastoma tumours. *Expert Rev Mol Med.* 2008;10.
18. Sitohy B, Nagy JA, Jaminet SCS, Dvorak HF. Tumor-surrogate blood vessel subtypes exhibit differential susceptibility to anti-VEGF therapy. *Cancer Res.* 2011;71(22):7021–7028. doi:10.1158/0008-5472.CAN-11-1693
19. Lamszus K, Brockmann MA, Eckerich C, et al. Inhibition of glioblastoma angiogenesis and invasion by combined treatments directed against vascular endothelial growth factor Receptor-2, epidermal growth factor receptor, and vascular endothelial-cadherin. *Clin Cancer Res.* 2005;11(13):4934–4940. doi:10.1158/1078-0432.CCR-04-2270
20. Kessel DH, Bhuvaneshwari R, Gan YY, et al. Combination of angiogenesis inhibitors increases the anti-tumor efficacy of photodynamic therapy in a human bladder tumor xenograft model. *Int Soc Optics Photonics.* 2009;7380:73806D.
21. Chen CH, Wu YJ, Chen JJ. Photo-thermal therapy of bladder cancer with Anti-EGFR antibody conjugated gold nanoparticles. *Front Biosci.* 2016;21(6):1211–1221. doi:10.2741/4451
22. Kraus D, Palasuberniam P, Chen B. Targeting phosphatidylinositol 3-kinase signaling pathway for therapeutic enhancement of vascular-targeted photodynamic therapy. *Mol Cancer Ther.* 2017. 16(11):2422–2431.
23. Li X, Carmeliet P. Targeting angiogenic metabolism in disease. *Science.* 2018;359(6382):1335–1336. doi:10.1126/science.aar5557
24. Huang F, Hurlburt W, Greer A, et al. Differential mechanisms of acquired resistance to insulin-like growth Factor-I receptor antibody therapy or to a small-molecule inhibitor, BMS-754807, in a human rhabdomyosarcoma model. *Cancer Res.* 2010;70(18):7221–7231. doi:10.1158/0008-5472.CAN-10-0391
25. Kesharwani SS, Kaur S, Tummala H, Sangamwar AT. Multifunctional approaches utilizing polymeric micelles to circumvent multidrug resistant tumors. *Colloid Surf B.* 2019;173:581–590. doi:10.1016/j.colsurfb.2018.10.022
26. Kargiotis O, Rao JS, Kyritsis AP. Mechanisms of angiogenesis in gliomas. *J Neurooncol.* 2006;78(3):281–293. doi:10.1007/s11060-005-9097-6
27. Parthymou A, Kardamakis D, Pavlopoulos I, Papadimitriou E. Irradiated C6 glioma cells induce angiogenesis in vivo and activate endothelial cells in vitro. *Int J Cancer.* 2004;110(6):807–814. doi:10.1002/(ISSN)1097-0215 doi.org/10.1002/ijc.20188
28. Xu W, Luo, Li, Zhou C, Cui D, Pang, Qiushi R, Fu S. RGD-conjugated gold nanorods induce radiosensitization in melanoma cancer cells by downregulating α v β 3 expression. *Int J Nanomedicine.* 2012;9:15. doi:10.2147/IJN.S28314
29. Takano S, Tsuboi K, Tomono Y, Mitsui Y, Nose T. Tissue factor, osteopontin, α v β 3 integrin expression in microvasculature of gliomas associated with vascular endothelial growth factor expression. *Br J Cancer.* 2000;82(12):1967–1973.
30. Zhou Y, Kim Y-S, Chakraborty S, Shi J, Gao H, Liu S. 99mTc-labeled cyclic RGD peptides for noninvasive monitoring of tumor integrin α v β 3 expression. *Mol Imaging.* 2011;10(5):7290.2011.00006. doi:10.2310/7290.2011.00006
31. Zhang P, Hu L, Yin Q, Feng L, Li Y. Transferrin-modified c[RGDFK]-paclitaxel loaded hybrid micelle for sequential blood-brain barrier penetration and glioma targeting therapy. *Mol Pharm.* 2012;9(6):1590–1598. doi:10.1021/mp200600t
32. Jheng P-R, Lu K-Y, Yu S-H, Mi F-L. Free DOX and chitosan- N - arginine conjugate stabilized indocyanine green nanoparticles for combined chemophotothermal therapy. *Colloids Surf B.* 2015;136:402–412. doi:10.1016/j.colsurfb.2015.09.032
33. Zheng C, Zheng M, Gong P, et al. Indocyanine green-loaded biodegradable tumor targeting nanoprobe for in vitro and in vivo imaging. *Biomaterials.* 2012;33(22):5603–5609. doi:10.1016/j.biomaterials.2012.04.044
34. Yan F, Wu H, Liu H, et al. Molecular imaging-guided photothermal/ photodynamic therapy against tumor by iRGD-modified indocyanine green nanoparticles. *J Controlled Release.* 2016;224:217–228. doi:10.1016/j.jconrel.2015.12.050
35. Wang H, Li X, Tse BW-C, et al. Indocyanine green-incorporating nanoparticles for cancer theranostics. *Theranostics.* 2018;8(5):1227–1242. doi:10.7150/thno.22872
36. Xu F, Liu M, Li X, et al. Loading of indocyanine green within polydopamine-coated laponite nanodisks for targeted cancer photothermal and photodynamic therapy. *Nanomaterials.* 2018;8(5):347. doi:10.3390/nano8050347
37. Du Y-Z, Cai -L-L, Liu P, You J, Yuan H, Hu F-Q. Tumor cells-specific targeting delivery achieved by A54 peptide functionalized polymeric micelles. *Biomaterials.* 2012;33(34):8858–8867. doi:10.1016/j.biomaterials.2012.08.043
38. Liu N, Tan Y, Hu Y, et al. A54 peptide modified and redox-responsive glucolipid conjugate micelles for intracellular delivery of doxorubicin in hepatocarcinoma therapy. *ACS Appl Mater Interfaces.* 2016;8(48):33148–33156. doi:10.1021/acsami.6b09333
39. Hu Y-W, Du Y-Z, Liu N, et al. Selective redox-responsive drug release in tumor cells mediated by chitosan based glycolipid-like nanocarrier. *J Controlled Release.* 2015;206:91–100. doi:10.1016/j.jconrel.2015.03.018

40. Meng T, Liu J, Wen L, et al. Multi-cycle chemotherapy with the glycolipid-like polymeric micelles evade cancer stem cell enrichment in breast cancer therapy. *Oncotarget*. 2016;7(45):72978–72989. doi:10.18632/oncotarget.v7i45
41. Atilgan S, Ekmekci Z, Dogan AL, Guc D, Akkaya EU. Water soluble distyryl-boradiazaindacenes as efficient photosensitizers for photodynamic therapy. *Chem Commun*. 2006;42:4398. doi:10.1039/b612347c
42. Vankayala R, Lin -C-C, Kalluru P, Chiang C-S, Hwang KC. Gold nanoshells-mediated bimodal photodynamic and photothermal cancer treatment using ultra-low doses of near infra-red light. *Biomaterials*. 2014;35(21):5527–5538. doi:10.1016/j.biomaterials.2014.03.065
43. Wen L, Tan Y, Dai S, et al. VEGF-mediated tight junctions pathological fenestration enhances doxorubicin-loaded glycolipid-like nanoparticles traversing BBB for glioblastoma-targeting therapy. *Drug Delivery*. 2017;24:1843–1855.

International Journal of Nanomedicine

Dovepress

Publish your work in this journal

The International Journal of Nanomedicine is an international, peer-reviewed journal focusing on the application of nanotechnology in diagnostics, therapeutics, and drug delivery systems throughout the biomedical field. This journal is indexed on PubMed Central, MedLine, CAS, SciSearch®, Current Contents®/Clinical Medicine,

Journal Citation Reports/Science Edition, EMBase, Scopus and the Elsevier Bibliographic databases. The manuscript management system is completely online and includes a very quick and fair peer-review system, which is all easy to use. Visit <http://www.dovepress.com/testimonials.php> to read real quotes from published authors.

Submit your manuscript here: <https://www.dovepress.com/international-journal-of-nanomedicine-journal>